Analysis of Stereochemical Stability of Dynamic Chiral Molecules using an Automated Microflow Measurement System

Igawa, Kazunobu
Institute for Materials Chemistry and Engineering, IRCCS

Asano, Shusaku
Institute for Materials Chemistry and Engineering, IRCCS

Yoshida, Yuki
Department of Molecular and Material Sciences, Kyushu University

Kawasaki, Yuuya
Institute for Materials Chemistry and Engineering, IRCCS

他

出版情報：The Journal of Organic Chemistry. 86 (14), pp.9651-9657, 2021-07-16. American Chemical Society
バージョン：
権利関係：

Analysis of Stereochemical Stability of Dynamic Chiral Molecules using an Automated Microflow Measurement System

Kazunobu Igawa,*[,†,‡] Shusaku Asano,*[,†] Yuki Yoshida,[‡] Yuuya Kawasaki,[†] and Katsuhiko Tomooka *[,†,‡]

[†]Institute for Materials Chemistry and Engineering, IRCCS, and [‡]Department of Molecular and Material Sciences, Kyushu University, Kasuga, Fukuoka 816-8580, Japan

*E-mail: kigawa@cm.kyushu-u.ac.jp, shusaku_asano@cm.kyushu-u.ac.jp, ktomooka@cm.kyushu-u.ac.jp

Dynamic Chiral Molecules, Racemization Rate, Microflow Measurement, Planar Chirality, Axial Chirality

ABSTRACT: An automated microflow measurement system for the kinetic study of racemization of dynamic chiral molecules was developed. This system facilitated the analysis of fast racemization within several seconds at elevated temperatures owing to its rapid heating ability, high performance for controlling short residence times, and ease of connection to HPLC systems for direct measurement of the enantiomeric purity. A more precise analysis was realized by combination of microflow and common batch measurements over a broad range of temperatures.

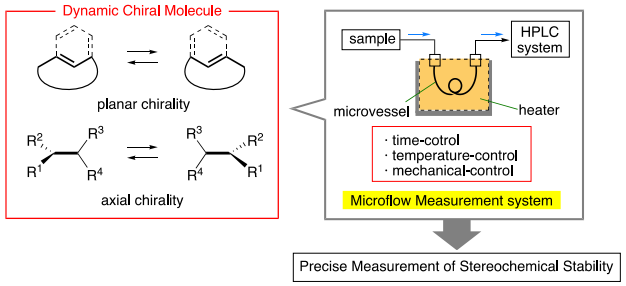

INTRODUCTION

Studies on the structure and synthesis of chiral molecules have been one of the most fundamental research areas in organic chemistry.[1] The main subject in this field is chiral molecules having asymmetric carbons, which are ubiquitous in nature. Chiral molecules having central chirality are stereochemically static, i.e., their enantiomers are not mutually convertible without bond dissociation and recombination.

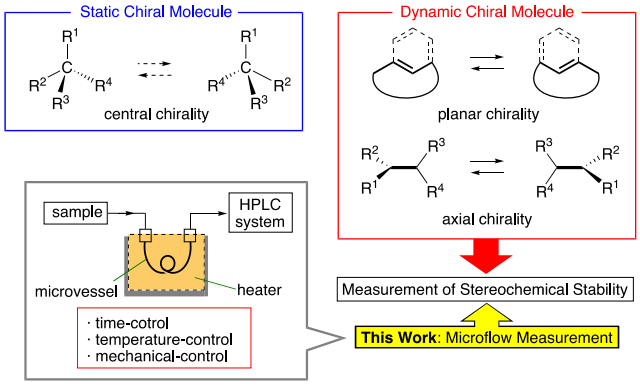

Figure 1. Classification of chiral molecules and outline of this work.

On the other hand, it is well known that other types of chiral molecules are capable of interconverting their enantiomers upon rotation of the σ bonds without bond dissociation and recombination. These are classified as dynamic chiral molecules (DYCMs), which are represented by planar and axial chiral molecules, as shown in Figure 1.[2-5] The stereochemical stability of DYCMs highly depends on the presence/absence, position and difference of substituents, as well as the type and number of constituent elements of the molecular skeleton. To elucidate the stereochemical behavior of DYCMs, we have developed a novel automated microflow measurement system that enabled rapid and easy measurements of time-dependent changes in the optical activity of DYCMs by connecting a microvessel to an HPLC system. In this system, a microvessel was used to achieve precise control of time and temperature for the racemization of DYCMs, not for the operation of reactions like as microflow reactors.[6] Herein, we describe the advantages and detailed features of this microflow measurement system for the study on the chemistry of DYCMs.

The analysis of the stereochemical stability of DYCMs is a fundamental and important issue, which is quantified by the activation parameters of racemization (activation Gibbs energy: $\Delta G_{rac}^{\ddagger}$, activation enthalpy: $\Delta H_{rac}^{\ddagger}$, and activation entropy: $\Delta S_{rac}^{\ddagger}$) obtained by the Eyring plots of several kinetic constant values of racemization (k_{rac}) at different temperatures. To determine the parameters, observation methods

for time/temperature dependent changes of the enantiomeric distribution in a racemization process have been well performed by using dynamic NMR spectroscopy and dynamic HPLC.[7] More immediate method for monitoring of the racemization of isolable enantiomers of DYCMs is the measurement of enantiomeric excess values of samples in a batch vessel using an HPLC with chiral stationary phase (chiral HPLC)[8] while maintaining a constant temperature in several times at different temperatures, which is laborious. The appropriate range of half-lives of optical activity ($_{opt}t_{1/2} = \ln 2 \cdot k_{rac}^{-1}$) for batch measurement is a few tens of minutes (e.g., 30 min [5.0×10^{-1} h]) to several weeks (e.g., 4 weeks [6.7×10^{2} h]) for a precise and practical measurement, as represented by the blue-colored cells in Figure 2a.[9] Another limitation of this method is that the measured temperatures should be below the boiling points of the used solvents to avoid changes in the concentration and temperature upon evaporation of the solvent. Low-temperature measurements (e.g., below 0 °C) are also inappropriate as they are easily affected by the racemization caused by the elevated temperature during the injection operations for the chiral HPLC analysis at ambient temperature. Therefore, the temperature range of the batch measurement is insufficient to obtain precise activation parameters from the Eyring plot.[10] In particular, evaluation of $\Delta S_{rac}^{\ddagger}$ is not accurate in a short temperature range, which is provided by extrapolated value of ln (k_{rac}/T) at virtual $1/T = 0$ from the obtained line by the Eyring plots (Figure 2b). To solve this fundamental problem, we designed an automated measurement method using a microflow system. The appropriate $_{opt}t_{1/2}$ value of the DYCMs for the microflow system ranged from a few seconds (e.g., 5 s [1.4×10^{-3} h]) to a few minutes (e.g., 5 min [8.3×10^{-2} h]), as indicated by the red-colored cells in Figure 2a. The measurements could be performed at temperatures higher than the boiling point of the solvents at ambient pressure using a back pressure valve (BPV). Moreover, the microflow measurement system has advantages such as short measurement times and possibility of full automation by computer control.

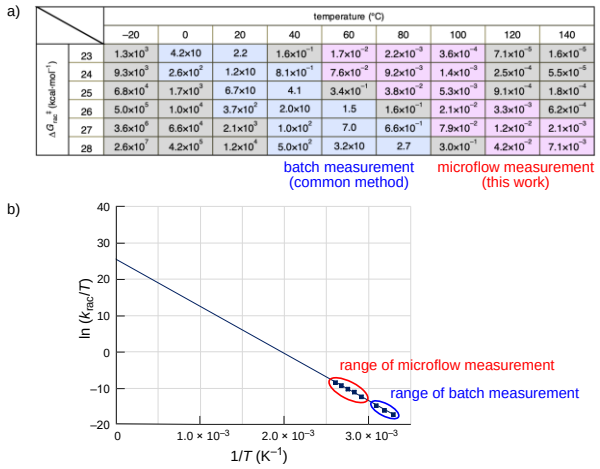

Figure 2. a) Appropriate range of batch measurement and microflow measurement. b) An example of Eyring plot (same as Figure 10) with indications of ranges of the measurement methods.

Furthermore, the combination of the microflow measurement system with the common batch measurement enabled the acquisition of highly accurate Eyring plot over a broad range of measurement temperatures (blue- and red-colored cells in Figure 2a). In this study, we analyzed the stereochemical behavior of nitrogen containing orthocyclophene **1** [11] and 2,6-disubstituted *N*-arylamide **2** [12] using the novel microflow measurement system combined with batch measurements (Figure 3).

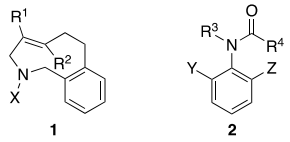

Figure 3. Structure of orthocyclophene **1** and *N*-arylamide **2**.

RESULTS AND DISCUSSION

We assembled a 20 μL stainless steel (SS) sample loop (internal diameter: 170 μm) as the microvessel, and an oil bath was used as the heating media (Figure 4). The heating time of the sample in the microvessel was identical to the residence time of the fluid at a controlled temperature, which was regulated by changing the flow rate and bath temperature. The outlet of the microvessel was connected to a shell-in-tube-type heat exchanger (HE, internal diameter of the inner tube: 100 μm) for securing an efficient cooling of the sample to prevent decrease of enantiomeric purity. The end of the HE was connected to an automatic injector with a 5 μL SS sample loop and a BPV at 6.9 bar. An SS syringe and syringe pump were used for precise sample feeding under high pressure conditions. The flow rate, temperature of the oil bath, and sample injection were automatically controlled using a bespoke software,[13] which performed a stepwise operation based on predefined measurement conditions in an input spreadsheet file. The feeding time for each condition was set to be five times longer than the residence time in the microvessel to obtain a steady state of the flow system.

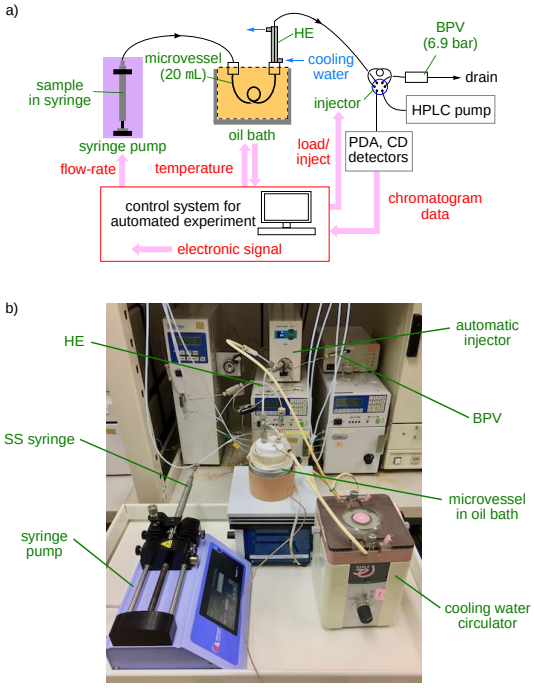

Figure 4. a) Outline of the microflow measurement system. b) Photograph of the microflow measurement system.

The sample in the loop of the automatic injector was injected into the HPLC system, and the sample feeding was stopped during temperature control for the next measurement according to the input file. The HPLC system was equipped with a common photodiode array (PDA) detector and a circular dichroism (CD) detector that is useful for the detection of chiral molecules.

At the outset, we performed a kinetic study on the racemization of orthocyclophene **1**, which was previously designed as a new class of planar chiral heterocycles and utilized as a chiral building block for nitrogen-containing chiral molecules.[11a] The stereochemical stability of **1** strongly depended on the presence/absence, position and difference of substituents at the E-alkene moiety. In the previous work, we synthesized **1a** (R^1 = H, R^2 = H, X = Ts in Figure 3) and measured its racemization rate in hexane by batch measurement at 40, 50, and 60 °C, providing ${}_{opt}t_{1/2}$ values 6.9, 1.9 h, and 33 min, respectively (Figure 5 and Figure 6c, entries 1-3).[11a] The Eyring plot provided activation parameters of $\Delta H_{rac}^{\ddagger}$ = 25.5 kcal·mol–1 and $\Delta S_{rac}^{\ddagger} = 5.46 \times 10^{-1}$ cal·mol^{-1}·K^{-1}; thus, the $\Delta G_{rac}^{\ddagger}$ at 25 °C was 25.3 kcal·mol^{-1}.[11a]

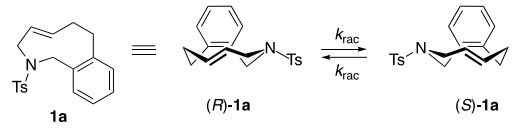

Figure 5. Structure and stereochemical behavior of orthocyclophene **1a**.

Herein, we performed a kinetic study of **1a** in hexane with a microflow system at 60, 90, 100, 110, and 120 °C. The residence times of the microflow system were corrected using the coefficient of thermal expansion of hexane,[14] which shortened the residence times in the heated microvessel. For an example, overlapping chiral HPLC chromatogram of **1a** at 120 °C with a CD detector is shown in Figure 6a.[15] The plot of ln(ee/ee_0), where ee is the observed enantiomeric excess value and ee_0 is its initial value, against time exhibited a straight line at all temperatures (Figure 6b). The kinetic constants for the decrease in enantiomeric excess k' (= $2k_{rac}$) were obtained from the slopes of the straight lines. The ${}_{opt}t_{1/2}$ values at 90, 100, 110, and 120 °C were 42.6, 16.3, 7.39, and 3.10 s, respectively, with a minimal standard errors (SE) below ±2.1% (Figure 6c, entries 5-8). The ${}_{opt}t_{1/2}$ values changed by 8,000 times upon a temperature difference of 80 °C, as they were 6.9 h and 3.1 s at 40 and 120 °C, respectively. In contrast, the ${}_{opt}t_{1/2}$ value at 60 °C was 16.4 min with a large SE (±6.5%) (Figure 6c, entry 4), which was approximately half of the previously reported value provided by a batch measurement (Figure 6c, entry 3). In this regard, we will discuss in detail later.

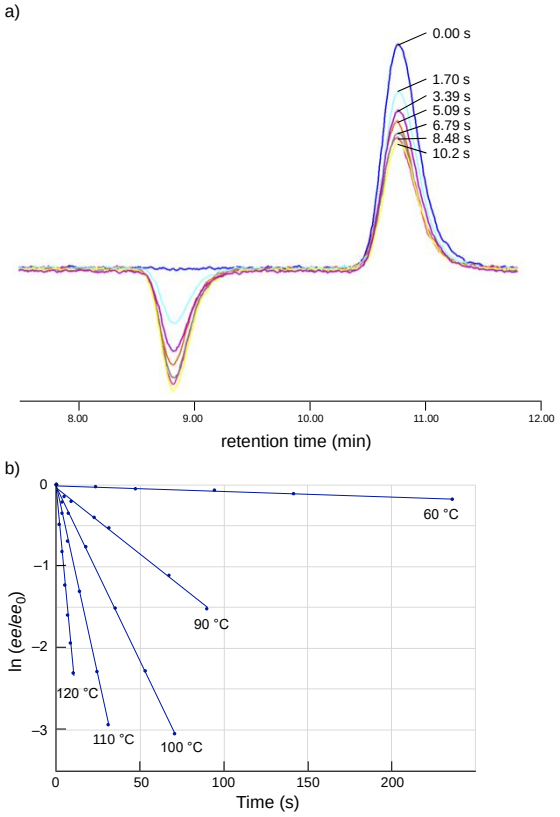

c)

Entry	Temp (°C)	Vessel	k' (s^{-1})	SE (%)	${}_{opt}t_{1/2}$
1 [11a]	40	batch	2.80×10^{-5}	–	6.9 h
2 [11a]	50	batch	1.03×10^{-4}	–	1.9 h
3 [11a]	60	batch	3.48×10^{-4}	–	33 min
4	60	microflow	$7.03(46) \times 10^{-4}$	± 6.5	16.4(11) min
5	90	microflow	$1.63(3) \times 10^{-2}$	± 2.1	42.6(9) s
6	100	microflow	$4.27(4) \times 10^{-2}$	± 0.91	16.3(1) s
7	110	microflow	$9.38(6) \times 10^{-2}$	± 0.62	7.39(5) s
8	120	microflow	$2.23(4) \times 10^{-1}$	± 2.0	3.10(6) s

Figure 6. Kinetic analysis of the racemization of **1a**; a) Overlapping chiral HPLC chromatogram of **1a** provided by a microflow measurement at 120 °C with a CD detector [IG (4.6 ϕ × 25 cm), *n*-hexane/*i*-PrOH = 30:70, flow rate = 1.0 mL/min, λ = 254 nm, 25 °C] . b) Plot for the first-order kinetics in second by using the microflow measurement. c) Provided kinetic constants and ${}_{opt}t_{1/2}$ depending on the temperature.

The Eyring plot for the racemization of **1a** were obtained from the reported data at 40, 50, and 60 °C (Figure 6c, entries 1-3) as well as 90, 100, 110, and 120 °C (Figure 6c, entries 5-8), which were determined by using the batch measurement and automated flow system, respectively (Figure 7). The Eyring plot displayed a straight line (R^2 = 0.9985) and activation parameters of $\Delta H_{rac}^{\ddagger}$ = 27.3 kcal·mol^{-1} and $\Delta S_{rac}^{\ddagger}$ = 6.38 cal·mol^{-1}·K^{-1};[14] thus $\Delta G_{rac}^{\ddagger}$ at 25 °C is 25.4 kcal·mol^{-1}.[16] The $\Delta H_{rac}^{\ddagger}$ and $\Delta S_{rac}^{\ddagger}$ values differed from the previously reported ones obtained from the batch measurement using three data points within an unreliable short range of temperatures. The combination of the microflow and batch measurements showed that the racemization of **1a** was enthalpy dominant with a small positive activation entropy.

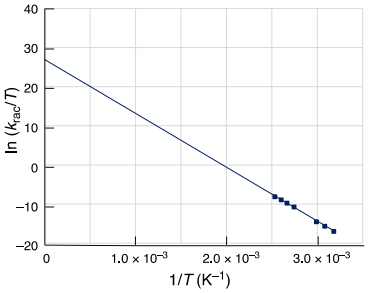

Figure 7. Eyring plots for the racemization of **1a** with kinetic constants in the range from 40 to 120 °C (R^2 = 0.9985).

Above mentioned large SE of microflow measurement at 60 °C (Figure 6c, entry 4) and the difference from the $_{opt}t_{1/2}$ values of batch measurement at that temperature may be caused by following reasons for errors on the microflow measurement. 1) When a long measurement time is required, the flow rate becomes too small causing back mixing by molecular diffusion results in an inaccurate residence time. 2) Substantial background racemization might proceed during the long operation time. 3) Shortening of measurement time to avoid the long operation time cause large SE values owing to the small change of enantiomeric purity as shown low slope line at 60 °C in Figure 6b. Therefore, appropriate $_{opt}t_{1/2}$ value as shown in red-colored cells in Figure 2a is important to apply the microflow measurement.

Next, we performed a kinetic study on the racemization of 2,6-disubstituted *N*-arylamide **2**,[12] which possessed a substantial rotational barrier depending on the steric hindrance of the substituents Y, Z, R^3, and R^4 in Figure 3 which caused the axial chirality at the C_{Ar}–N bond. It was found that **2a** (Y = OBn, Z = OH, R^3 = Bn, R^4 = CH=CHPh)[17] exhibits axial chirality and detectable racemization at 40 °C within a few hours after the separation of the enantiomers using a chiral HPLC (Fig. 8).

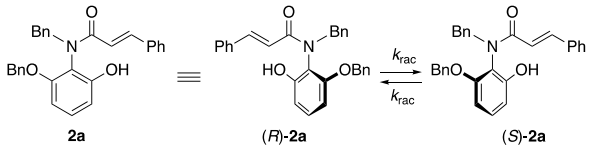

Figure 8. Structure and stereochemical behavior of *N*-arylamide **2a**.

Based on this observation, we performed a kinetic analysis of the racemization of **2a** in ethanol (Figure 9) by the automated microflow system at 70, 80, 90, 100, and 110 °C (Figure9a, 9b, and 9c, entries 4-8) with correction of the thermal expansion of ethanol,[18] along with batch measurement at 30, 40, and 50 °C (Figure 9a, and 9c, entries 1-3).[15] The $_{opt}t_{1/2}$ values also differed by 8,000 times upon a temperature difference of 80 °C, as they were found to be 8.92 h and 4.02 s at 30 and 110 °C, respectively (Figure 9c).

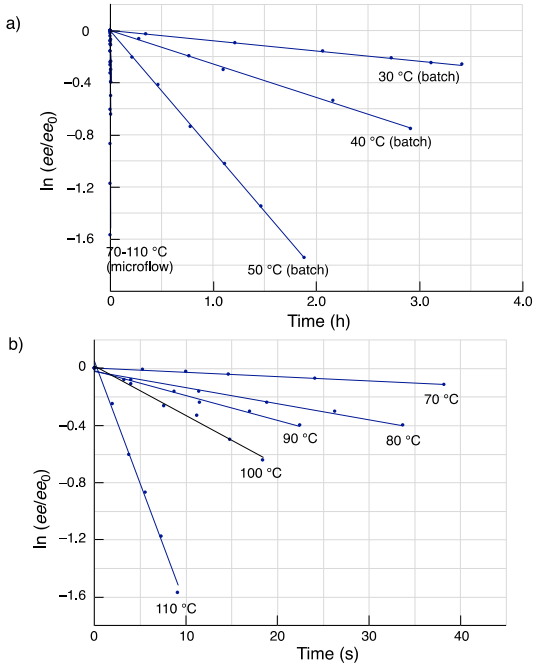

c)

Entry	Temp (°C)	Vessel	k' (s^{-1})	SE (%)	$_{opt}t_{1/2}$
1	30	batch	2.16(3) × 10^{-5}	± 1.3	8.92(12) h
2	40	batch	7.12(16) × 10^{-5}	± 2.2	2.71(6) h
3	50	batch	2.57(2) × 10^{-4}	± 0.6	45.0(3) min
4	70	microflow	3.07(12) × 10^{-3}	± 3.8	3.76(14) min
5	80	microflow	1.12(5) × 10^{-2}	± 4.9	1.03(5) min
6	90	microflow	2.86(5) × 10^{-2}	± 1.6	24.3(4) s
7	100	microflow	7.03(17) × 10^{-2}	± 2.4	9.86(24) s
8	110	microflow	1.72(7) × 10^{-1}	± 3.8	4.02(15) s

Figure 9. Kinetic analysis of the racemization of **2a**; a) Plot of the first-order kinetics in hour. b) Plot of the first-order kinetics in second. c) Provided kinetic constants and $_{opt}t_{1/2}$ depending on the temperature.

The combination of microflow and batch measurements provided the activation parameters ($\Delta H_{rac}^{\ddagger}$ = 25.7 kcal·mol^{-1}, $\Delta S_{rac}^{\ddagger}$ = 3.44 cal·mol^{-1}·K^{-1}) [19] by Eyring plot (Figure 10) with a corresponding $\Delta G_{rac}^{\ddagger}$ at 25 °C of 24.7 kcal·mol^{-1}, which showed that the racemization of **2a** is also enthalpy dominant with a small positive activation entropy.

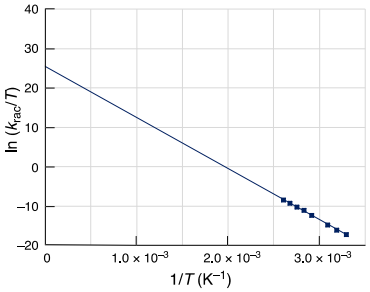

Figure 10. Eyring plot for the racemization of **2a** with kinetic constants in the range from 30 to 110 °C (R^2 = 0.9990).

CONCLUSIONS

In summary, we developed an automated microflow measurement system for the kinetic study of the racemization of DYCMs. This method facilitated the performance of quick and efficient kinetic studies at the second time scale

with high precision. The combination of the presented microflow system and common batch measurement resulted in a more reliable analysis of the Eyring plot over a broad range of temperatures. This new analytical approach to evaluate the stereochemical behavior of DYCMs allows to accelerate the understanding and application of DYCMs. Further improvement and validation of the microflow measurement system by application to a variety of DYCMs are in progress.

EXPERIMENTAL SECTION

General Methods. All reactions were carried out in heat-gun-dried glassware under an argon atmosphere unless otherwise noted. Dry THF was purchased from Kanto Chemical Co., Inc. and used without further purification. ^{1}H NMR, ^{13}C NMR spectra were recorded on a Varian Mercury (^{1}H: 300 MHz, ^{13}C: 75 MHz) at ambient temperature using $CDCl_3$ as solvents. Chemical shifts (δ) in ppm were referenced to the residual protonated solvent peak or deuterated solvent peak as an internal standard: $CHCl_3$ for ^{1}H NMR (δ 7.26) and $CDCl_3$ for ^{13}C NMR (δ 77.1). The peak multiplicities were given as followed: s, singlet; d, doublet; q, quartet; quin, quintet; m, multiplet; br, broad. Infrared spectra were recorded on a Fourier transfer infrared spectrophotometer (Perkin Elmer SpectrumOne) as neat liquid on NaCl plates or as crystals by use of a diffuse reflector. High performance liquid chromatography (HPLC) were performed on a JASCO CD-2095 and MD-2018 detectors equipped with a JASCO PU-2089 using Daicel CHIRALPAK IG column (0.46 cm × 25 cm), and semi-preparative CHIRALPAK IG column (2.0 cm × 25 cm). Analytical thin-layer chromatography (TLC) was carried out on silica gel 60 F_{254} (Merck 5715) plates and developed plates were visualized by UV (254 nm) and by heating on a hot plate after staining with a 4% solution of phosphomolybdic acid in ethanol or a 2.5% solution of *p*-anisaldehyde in ethanol. Column chromatography was performed using Fuji Silysia silica-gel FL100D (neutral). HRMS analyses were recorded on a JEOL JMS-700 at the Analytical Center in IMCE, Kyushu University. Unless otherwise noted, all reagents were purchased and used without further purification. Compound **1a** was synthesized according to our previous report.[10a] Compound **2a** was synthesized by original procedure from commercially available 2-nitroresorcinol as follows. The synthetic scheme for **2a** is shown in the Supporting Information.

3-((*tert*-butyldimethylsilyl)oxy)-2-nitrophenol (**3**). To a solution of 2-nitroresorcinol (1.00 g, 6.45 mmol) and imidazole (439 mg, 6.45 mmol) in THF (30 mL) was added TBSCl (972 mg, 6.45 mmol) at 0 °C. After stirred at ambient temperature for 2 h, the colorless suspended mixture was filtered through a pad of Celite using Et_2O. The filtrate was concentrated under reduced pressure and the residue was purified by silica gel chromatography (*n*-hexane/AcOEt = 95:5) to afford 1.21 g (70%) of **3** as a yellow oil. ^{1}H NMR (300 MHz, $CDCl_3$): δ 10.2–8.72 (br, 1H), 7.29 (dd, *J* = 8.5, 8.5 Hz, 1H), 6.68 (dd, *J* = 8.5, 1.5 Hz, 1H), 6.45 (dd, *J* = 8.5, 1.5 Hz, 1H), 1.01 (s, 9H), 0.26 (s, 6H). ^{13}C{^{1}H} NMR (75 MHz, $CDCl_3$): δ 155.3, 151.9, 135.3, 129.6, 112.5, 111.0, 25.8, 18.4, –4.3. IR (neat, cm^{-1}): 3429, 2933, 1588, 1539, 1364, 1220, 1122, 837, 786, 671. HRMS (FAB/double-focusing, matrix: 3-nitrobenzyl alcohol, positive) *m/z*: [M+H]$^+$ calcd for $C_{12}H_{20}NO_4Si$ 270.1162; found 270.1161.

***tert*-butyl(3-(methoxymethoxy)-2-nitrophenoxy)dimethylsilane (4)**. To a solution of **3** (1.21 g, 4.49 mmol) and Hünig base (1.86 mL, 10.8 mmol) in CH_2Cl_2 (20 mL) was added MOMCl (406 μL, 5.39 mmol) at 0 °C. After stirred at that temperature for 30 min, the reaction was quenched with H_2O and extracted with CH_2Cl_2. The combined organic phase was washed with brine, dried over Na_2SO_4, filtered and the filtrate was concentrated under reduced pressure. The residue was purified by silica gel chromatography (*n*-hexane/AcOEt = 95:5) to afford 1.07 g (76%) of **4** as a colorless oil. ^{1}H NMR (300 MHz, $CDCl_3$): δ 7.20 (dd, *J* = 8.7, 8.1 Hz, 1H), 6.82 (d, *J* = 8.1 Hz, 1H), 6.57 (d, *J* = 8.7 Hz, 1H), 5.20 (s, 2H), 3.47 (s, 3H), 0.95 (s, 9H), 0.24 (s, 6H). ^{13}C{^{1}H} NMR (75 MHz, $CDCl_3$): δ 149.5, 148.1, 135.9, 130.6, 113.1, 108.0, 94.9, 56.5, 25.4, 18.1, –4.5. IR (neat cm^{-1}): 2933, 1586, 1538, 1375, 1257, 1100, 1061, 833, 787, 672. HRMS (FAB/double-focusing, matrix: 3-nitrobenzyl alcohol, positive) *m/z*: [M+H]$^+$ calcd for $C_{14}H_{24}NO_5Si$ 314.1424; found 314.1424.

***N*-(2-((*tert*-butyldimethylsilyl)oxy)-6-(methoxymethoxy)phenyl)cinnamamide** (**5**). To a solution of **4** (1.02 g, 3.25 mmol) in MeOH (20 mL) was added 10% palladium on active charcoal (100 mg, 0.0941 mmol) at ambient temperature. The mixture was stirred for 24 h under ambient pressure of hydrogen at that temperature. The mixture was filtered through a pad of Celite using AcOEt, and the filtrate was concentrated under reduced. To a solution of the thus obtained crude product in THF (10 mL) was added pyridine (525 μL, 6.50 mmol) and cinnamoyl chloride (650 mg, 3.90 mmol) at 0 °C. After stirred at ambient temperature for 7 h, the reaction was quenched with sat. aq. NH_4Cl and extracted with CH_2Cl_2. The combined organic phase was washed with brine, dried over Na_2SO_4, filtered and the filtrate was concentrated under reduced pressure. The residue was purified by silica gel chromatography (*n*-hexane/AcOEt = 80:20) to afford 1.08 g (80% in 2 steps) of **5** as colorless crystals. ^{1}H NMR (300 MHz, $CDCl_3$): δ 7.72 (d, *J* = 15.6 Hz, 1H), 7.54–7.41 (br, 2H), 7.41–7.28 (m, 3H), 7.10 (dd, *J* = 8.2, 8.2 Hz, 1H), 6.83 (dd, *J* = 8.2, 1.2 Hz, 1H), 6.71–6.48 (br, 1H), 6.61 (dd, *J* = 8.2, 1.2 Hz, 1H), 5.16 (s, 2H), 3.43 (s, 3H), 0.96 (s, 9H), 0.19 (s, 6H). ^{13}C{^{1}H} NMR (75 MHz, $CDCl_3$): δ 164.2, 153.8, 151.8, 141.7, 135.0, 129.6, 128.8, 127.9, 127.5, 120.6, 118.4, 113.4, 108.5, 95.1, 56.2, 25.6, 18.1, –4.37. IR (reflection, cm^{-1}): 3234, 2929, 1662, 1468, 1347, 1253, 1155, 1053, 835, 783, 713. HRMS (EI/double-focusing, positive) *m/z*: [M]$^+$ calcd for $C_{23}H_{31}NO_4Si$ 413.2022; found 413.2021. Mp: 123.0-124.5 °C.

***N*-(2-hydroxy-6-(methoxymethoxy)phenyl)cinnamamide** (**6**). To a solution of **5** (931 mg, 2.25 mmol) in THF (5 mL) was added TBAF (ca. 1 M in THF, 2.25 mL, ca. 2.25 mmol) at ambient temperature. After stirred at that temperature for 30 min, the mixture was concentrated under reduced pressure. The residue was purified by silica gel chromatography (*n*-hexane/AcOEt = 10:90) to afford 656 mg (98%) of **6** as pale yellow crystals. ^{1}H NMR (300 MHz, $CDCl_3$): δ 10.4–10.1 (br, 1H), 8.26–8.10 (br, 1H), 7.78 (d, *J* = 15.2 Hz, 1H), 7.57–7.52 (m, 2H), 7.42–7.39 (m, 2H), 7.04 (dd, *J* = 8.2, 8.2 Hz, 1H), 6.74 (dd, *J* = 8.7, 1.2 Hz, 1H), 6.72 (dd, *J* = 8.1, 1.2 Hz, 1H), 6.68 (d, *J* = 15.2 Hz, 1H), 5.25 (s, 2H), 3.51 (s, 3H). ^{13}C{^{1}H} NMR (75 MHz, $CDCl_3$): δ 165.4, 150.0, 148.8, 144.2, 134.2, 130.5, 129.0, 128.2, 126.9, 118.9, 116.3, 113.9, 105.6, 95.6, 56.6. IR (reflection, cm^{-1}): 3304, 1480, 999, 861, 767. HRMS (EI/double-focusing, positive) *m/z*: [M]$^+$ calcd for $C_{17}H_{17}NO_4$ 299.1158; found 299.1158. Mp: 118.5-119.0 °C.

***N*-benzyl-*N*-(2-(benzyloxy)-6-(methoxymethoxy)phenyl)cinnamamide** (**7**). To a solution of **6** (299 mg, 1.00 mmol) in THF (2 mL) was added NaH (63% in mineral oil, 152 mg, 4.00 mmol) and BnBr (356 μL, 3.00 mmol) at 0 °C. After stirred at 60 °C for 12 h, the reaction was quenched with sat. aq. NH_4Cl and extracted with AcOEt. The combined organic phase was washed with brine, dried over Na_2SO_4, filtered and the filtrate was concentrated under reduced pressure. The residue was purified by silica gel chromatography (*n*-hexane /AcOEt = 85:15) to afford 450 mg (94%) of **7** as pale yellow oil. ^{1}H NMR (300 MHz, $CDCl_3$): δ 7.74 (d, *J* = 15.2 Hz, 1H), 7.31–7.11 (m, 15H), 6.76 (dd, *J* = 8.4, 1.2 Hz, 1H), 6.60 (dd, *J* = 9.0, 1.2 Hz, 1H), 6.36 (d, *J* = 15.8 Hz, 1H), 5.04 (d, *J* = 14.1 Hz, 1H), 4.97 (d, *J* = 12.3 Hz, 1H), 4.91 (d, *J* = 6.9 Hz, 1H), 4.90 (d, *J* = 14.1 Hz, 1H), 4.89 (d, *J* = 12.3 Hz, 1H), 4.85 (d, *J* = 6.9 Hz, 1H), 3.24 (s, 3H). ^{13}C{^{1}H} NMR (75 MHz, $CDCl_3$): δ 167.0, 155.6, 154.8, 141.8, 137.7, 136.6, 135.5, 129.6, 129.4, 129.3, 128.7, 128.5, 127.8, 127.8, 127.7, 127.0, 126.8, 119.7, 119.0, 107.6, 106.5, 94.5, 70.2, 56.1, 51.0. IR (neat, cm^{-1}): 3029, 1655, 1618, 1474, 1387, 1255, 1155, 1064, 923, 783, 763. HRMS (EI/double-focusing, positive) *m/z*: [M]$^+$ calcd for $C_{31}H_{29}NO_4$ 479.2097; found 479.2097.

***N*-benzyl-*N*-(2-(benzyloxy)-6-hydroxyphenyl)cinnamamide** (**2a**). To a solution of **7** (445 mg, 0.928 mmol) in MeOH (10 mL) was added conc. HCl (35-37%, 3 mL) at ambient temperature.

After stirred at that temperature for 15 h, the mixture was concentrated under reduced pressure and azeotrope with CH_3CN to afford 381 mg (94%) of **2a** as colorless crystals. The analytical data of **2a** were collected after purification by silica gel chromatography (*n*-hexane /AcOEt = 85:15). ^{1}H NMR (300 MHz, $CDCl_3$): δ 7.75 (d, *J* = 15.8 Hz, 1H), 7.29–7.10 (m, 16H), 6.67 (dd, *J* = 8.2, 8.2 Hz, 1H), 6.37 (d, *J* = 6.5 Hz, 1H), 6.34 (d, *J* = 15.8 Hz, 1H), 5.04 (d, *J* = 13.9 Hz, 1H), 4.93 (d, *J* = 13.9 Hz, 1H), 4.80 (d, *J* = 12.3 Hz, 1H), 4.71 (d, *J* = 12.3 Hz, 1H). ^{13}C{^{1}H} NMR (75 MHz, $CDCl_3$): δ 168.5, 155.5, 154.1, 143.1, 137.3, 136.6, 135.0, 129.9, 129.6, 129.6, 128.6, 128.5, 128.3, 127.9, 127.7, 127.6, 126.6, 118.4, 117.1, 109.7, 104.2, 69.9, 51.4. IR (reflection, cm^{-1}): 3078, 1645, 1093, 1018, 977, 906, 860. HRMS (EI/double-focusing, positive) *m*/*z*: [M]$^+$ calcd for $C_{29}H_{25}NO_3$ 435.1834; found 435.1834. Mp: 164.6-165.2 ℃. Analytical HPLC [IG (4.6 ϕ × 25 cm), *n*-hexane/*i*-PrOH = 50:50, flow rate = 1.0 mL/min, λ = 254 nm, 25 ℃]: t_1 = 5.5 min, t_2 = 8.5 min. Semi-preparative HPLC [IG (20 ϕ × 25 cm), *n*-hexane/EtOH = 60:40, flow rate = 8.0 mL/min, λ = 254 nm, 25 ℃]: t_1 = 12.6 min, t_2 = 17.6 min.

Detail of microflow measurement system. A SS syringe (8 mL volume, Harvard Apparatus) was used with a syringe pump (Pump Elite 11, Harvard Apparatus) for accurate liquid handling. USB-B cable was used for controlling the syringe pump from a bespoke software. PFA tube (2.18 mm i.d. 1/8 o.d., Nippon Pillar Packing) was used for the shell of the heat exchanger. 1/8" SS tees (Swagelok) were used with rubber septa for making the shell-in-tube structure. An automatic 6-port valve (VA-11-65-G, GL Sciences) was equipped with a BPV (100 psi, IDEX Health & Sciences). A jam jar filled with silicone oil was used as a miniature oil bath. A tape heater with 100 W capacity was used for heating the miniature oil bath from outside. A magnetic stirrer was used for keeping the bath temperature uniform. TC-01 thermometer (National Instruments) with a J-type thermocouple was used for temperature measurement. A switching module made of photo MOS relays (AQZ207, Panasonic) and a USB I/O device (USB-6001, National Instruments) controlled the valve rotation and heater power. A built-in PID algorithm in the bespoke software controlled the power of a tape heater based on the temperature input. A stable bath temperature with a maximum error of ±0.1 °C can be achieved with the help of the PID algorithm.

ASSOCIATED CONTENT

Supporting Information

The Supporting Information is available free of charge on the ACS Publications website.

Analytical data for stereochemical stability of DYCMs, synthetic scheme for compound **2a**, and NMR spectra for newly reported compounds (PDF).

AUTHOR INFORMATION

Corresponding Authors

Kauznobu Igawa
Shusaku Asano
Katsuhiko Tomooka

Author Contributions

K. Igawa: conceptualization of this work and writing original draft; S. Asano: development of methodology of microflow system and software; Y. Yoshida and Y. Kawasaki: performing experiments; K. Igawa and K. Tomooka: project administration; All authors: review and editing of draft.

ORCID

Kazunobu Igawa: 0000-0002-7354-5162
Shusaku Asano: 0000-0001-6297-057X
Yuuya Kawasaki: 0000-0003-3354-1690
Katsuhiko Tomooka: 0000-0002-0762-5746

Notes

The authors declare no competing financial interest.

ACKNOWLEDGMENT

This research was supported by JSPS KAKENHI Grants (20H02743, 20H05677, 20K15081) and the Cooperative Research Program of "Network Joint Research Center for Materials and Devices". This work was carried out by using the research equipment shared in the MEXT Project for promoting the public utilization of advanced research infrastructure (Program for supporting the introduction of the new sharing system), Grant Number JPMXS0422300120. The authors thank Yukiko Irie for her technical assistance.

REFERENCES

(1) (a) Kagan, H. *La Stéréochimie Organique*; Presses Universitaires de France: Paris, 1975. (b) *Asymmetric Synthesis, Vol 1-5*; Morrison, J. D., Ed.; Academic Press: New York, 1983-1985. (c) Eliel, E. L.; Wilen, S. H. *Stereochemistry of Organic Compounds*; Wiley: New York, 1994. (d) *Comprehensive Chirality*, *Vol. 1-9*; Carreira, E. M.; Yamamoto, H., Eds.; Elsevier: Amsterdam, 2012.

(2) For representative reviews on DYCMs, see: (a) Ōki, M. *The Chemistry of Rotational Isomers*; Springer: New York, 1993. (b) Wolf, C. *Dynamic Stereochemistry of Chiral Compounds: Principles and Applications*; RSC Publishing: Cambridge, 2008. (c) Mancinelli, M.; Bencivenni, G.; Pecorari, D.; Mazzanti, A., Stereochemistry and Recent Applications of Axially Chiral Organic Molecules. *Eur. J. Org. Chem.* **2020**, 4070-4086.

(3) For representative examples of synthetic applications of DYCMs, see: (a) Bringmann, G.: Jansen, J. R.; Rink, H.-P., Regioselective and Atropoisomeric-selective Aryl Coupling to give Naphthyl Isoquinoline Alkaloids: The First Total Synthesis of (–)-Ancistrocladine. *Angew. Chem. Int. Ed.* **1986**, *25*, 913-915. (b) Kawabata, T.; Yahiro, K.; Fuji, K., Memory of Chirality: Enantioselective Alkylation Reactions at an Asymmetric Carbon Adjacent to a Carbonyl Group. *J. Am. Chem. Soc.* **1991**, *113*, 9694-9696. (c) Oi, S.; Kawagoe, K.; Miyano, S., Acid-catalyzed Facile Racemization of Axially Dissymmetric 2'-Hydroxy-1,1'-binaphthyl-2-carboxylic Acid. *Chem. Lett.* **1993**, *22*, 79-80. (d) Bringmann, G.; Schöner, B.; Schupp, O.; Peters, K.; Peters, E. M.; Vonschnering, H. G., Synthesis, Optical Resolution, and Helimerization of Dinaphtho[2,1-b:1',2'-d]-pyran-4-one. *Liebigs Anna. Chem.* **1994**, 9191-9197. (e) Tomooka, K.; Komine, N.; Fujiki, D.; Nakai, T.; Yanagitsuru, S., Planar Chiral Cyclic Ether: Asymmetric Resolution and Chirality Transformation. *J. Am. Chem. Soc.* **2005**, *127*, 12182-12183. (f) Tomooka, K.; Suzuki, M.; Shimada, M.; Yanagitsuru, S.; Uehara, K., Planar Chiral Cyclic Amine and Its Derivatives: Synthesis and Stereochemical Behavior. *Org. Lett.* **2006**, *8*, 963-965. (g) Clayden, J.; Vallverdú, L.; Helliwell, M., Conformational Communication between the Ar-CO and Ar-N Axes in 2,2 '-Disubstituted Benzanilides and Their Derivatives. *Org. Biomol. Chem.* **2006**, *4*, 2106-2118. (h) Tomooka, K.; Suzuki, M.; Uehara, K.; Shimada, M.; Akiyama, T., Novel Synthetic Approach to Nine-Membered Diallylic Amides: Stereochemical Behavior and Utility as Chiral Building Block. *Synlett* **2008**, 2518-2522. (i) Tomooka, K.; Akiyama, T.; Man, P.; Suzuki, M., Asymmetric Synthesis of (–)- and (+)-Kainic Acid using a Planar Chiral Amide as a Chiral Building Block. *Tetrahedron Lett.* **2008**, *49*, 6327-6329; and references 11 and 12.

(4) Biological studies on DYCMs, see: (a) Takahashi, H.; Wakamatsu, S.; Tabata, H.; Oshitari, T.; Harada, A.; Inoue, K.; Natsugari,

H., Atropisomerism Observed in Indometacin Derivatives. *Org. Lett.* **2011**, *13*, 760-763. (b) Tabata, H.; Wada, N.; Takada, Y.; Nakagomi, J.; Miike, T.; Shirahase, H.; Oshitari, T.; Takahashi, H.; Natsugari, H., Active Conformation of Seven-membered-ring Benzolactams as New ACAT Inhibitors: Latent Chirality at *N*5 in the 1,5-Benzodiazepin-2-one Nucleus. *Chem. Eur. J.* **2012**, *18*, 1572-1576. (c) Selness, S. R.; Devraj, R. V.; Devadas, B.; Walker, J. K.; Boehm, T. L.; Durley, R. C.; Shieh, H.; Xing, L.; Rucker, P. V.; Jerome, K. D.; Benson, A. G.; Marrufo, L. D.; Madsen, H. M.; Hitchcock, J.; Owen, T. J.; Christie, L.; Promo, M. A.; Hickory, B. S.; Alvira, E.; Naing, W.; Blevis-Bal, R.; Messing, D.; Yang, J.; Mao, M. K.; Yalamanchili, G.; Embse, R. V.; Hirsch, J.; Saabye, M.; Bonar, S.; Webb, E.; Anderson, G.; Monahan, J. B., Discovery of PH-797804, a Highly Selective and Potent Inhibitor of p38 MAP Kinase. *Bioorg. Med. Chem. Lett.* **2011**, *21*, 4066-4071. (d) Wakamatsu, S.; Takahashi, Y.; Tabata, H.; Oshitari, T.; Tani, N.; Azumaya, I.; Katsumoto, Y.; Tanaka, T.; Hosoi, S.; Natsugari, H.; Takahashi, H., Conformation and Atropisomeric Properties of Indometacin Derivatives. *Chem. Eur. J.* **2013**, *19*, 7056-7063. (e) Sugane, T.; Tobe, T.; Hamaguchi, W.; Shimada, I.; Maeno, K.; Miyata, J.; Suzuki, T.; Kimizuka, T.; Sakamoto, S.; Tsukamoto, S.-I., Atropisomeric 4-Phenyl-4*H*-1,2,4-triazoles as Selective Glycine Transporter 1 Inhibitors. *J. Med. Chem.* **2013**, *56*, 5744-5756. For representative reviews on biological studies on DYCMs, see (f) Clayden, J.; Moran, W. J.; Edwards, P. J.; LaPlante, S. R., The Challenge of Atropisomerism in Drug Discovery. *Angew. Chem. Int. Ed.* **2009**, *48*, 6398-6401. (g) Glunz, P. W., Recent Encounters with Atropisomerism in Drug Discovery. *Bioorg. Med. Chem. Lett.* **2018**, *28*, 53-60.

(5) Recently, we have developed dynamic asymmetric induction (DYASIN) of DYCMs, which provides optically active DYCMs by interaction with outer chiral source, see: Igawa, K.; Kawasaki, Y.; Ano, Y.; Kashiwagi, T.; Ogawa, K.; Hayashi, J.; Morita, R.; Yoshioka, Y.; Uehara, K.; Tomooka, K., Preparation of Enantioenriched Chiral Organic Molecules by Dynamic Asymmetric Induction from a Outer Chiral Source. *Chem. Lett.* **2019**, *48*, 726-729.

(6) For representative reviews on microflow reactors, see: (a) Fukuyama, T.; Rahman, M. T.; Sato, M.; Ryu, I., Adventures in Inner Space: Microflow Systems for Practical Organic Synthesis. *Synlett* **2008**, 151-163. (b) Yoshida, J.-I.; Takahashi, Y.; Nagaki, A., Flash Chemistry: Flow Chemistry That cannot be done in Batch. *Chem. Commun.* **2013**, *49*, 9896-9904. (c) Plutschack, M. B.; Pieber, B.; Gilmore, K.; Seeberger, P. H., The Hitchhiker's Guide to Flow Chemistry(II). *Chem. Rev.* **2017**, *117*, 11796-11893. (d) Bloemendal, V.; Janssen, M.; van Hest, J. C. M.; Rutjes, F., Continuous One-flow Multistep Synthesis of Active Pharmaceutical Ingredients. *React. Chem. Eng.* **2020**, *5*, 1186-1197.

(7) For a review on dynamic NMR spectroscopy and dynamic HPLC analysis, see: Rickhaus, M.; Jundt, L.; Mayor M., Determining Inversion Barriers in Atropisomers – A Tutorial for Organic Chemists. *CHIMIA* **2016**, *70*, 192-202.

(8) For a review on chiral HPLC analysis, see: Okamoto, Y.; Ikai, T., Chiral HPLC for Efficient Resolution of Enantiomers. *Chem. Soc. Rev.* **2008**, *37*, 2593-2608.

(9) The values of half-live of optical activity were calculated by Eyring equation on the assumption that transmission coefficient is one.

(10) Uncertainty of activation parameters owing to the narrow thermal range of measurement was well discussed, see: Espenson, J. H. *Chemical Kinetics and Reaction Mechanisms, 2nd ed*; McGraw-Hill, Inc.: New York, 1995.

(11) (a) Tomooka, K.; Iso, C.; Uehara, K.; Suzuki, M.; Nishikawa-Shimono, R.; Igawa, K., Planar-chiral [7]Orthocyclophanes. *Angew. Chem. Int. Ed.* **2012**, *51*, 10355-10358. (b) Igawa, K.; Machida, K.; Noguchi, K.; Uehara, K.; Tomooka, K., Synthesis and Stereochemical Analysis of Planar-chiral (*E*)-4-[7]Orthocyclophene. *J. Org. Chem.* **2016**, *81*, 11587-11593.

(12) For representative studies on axial-chiral *N*-arylamides, see: (a) Curran, D. P.; Qi, H. Y.; Geib, S. J.; Demello, N. C., Atroposelective Thermal-Reactions of Axially Twisted Amides and Imides. *J. Am. Chem. Soc.* **1994**, *116*, 3131-3132. (b) Hughes, A. D.; Price, D. A.; Shishkin, O.; Simpkins, N. S., Diastereoselective Enolate Chemistry using Atropisomeric Amides. *Tetrahedron Lett.* **1996**, *37*, 7607-7610. (c) Kitagawa, O.; Izawa, H.; Taguchi, T.; Shiro, M., An Efficient Synthesis of Optically Active Axially Chiral Anilide and Its Application to Iodine-mediated Asymmetric Diels-Alder Reaction. *Tetrahedron Lett.* **1997**, *38*. 4447-4450. (d) Curran, D. P.; Liu, W. D.; Chen, C. H. T., Transfer of Chirality in Radical Cyclizations. Cyclization of *o*-Haloacrylanilides to Oxindoles with Transfer of Axial Chirality to a Newly Formed Stereocenter. *J. Am. Chem. Soc.* **1999**, *121*, 11012-11013. (e) Clayden, J.; McCarthy, C.; Helliwell, M., Bonded Peri-interactions Govern the Rate of Racemisation of Atropisomeric 8-Substituted 1-Naphthamides. *Chem. Commun.* **1999**, 2059-2060. (f) Adler, T.; Bonjoch, J.; Clayden, J. Font-Bardía, M.; Pickworth, M.; Solans, X.; Solé, D.; Vallverdú, L., Slow Interconversion of Enantiomeric Conformers or Atropisomers of Anilide and Urea Derivatives of 2-Substituted Anilines. *Org. Biomol. Chem.* **2005**, *3*, 3173-3183. (g) Guthrie, D. B.; Curran, D. P., Asymmetric Radical and Anionic Cyclizations of Axially Chiral Carbamates. *Org. Lett.* **2009**, *11*, 249-251. (h) Shirakawa, S.; Liu, K.; Maruoka, K., Catalytic Asymmetric Synthesis of Axially Chiral *o*-Iodoanilides by Phase-transfer Catalyzed Alkylations. *J. Am. Chem. Soc.* **2012**, *134*, 916-919. (i) Nakazaki, A.; Miyagawa, K.; Miyata, N.; Nishikawa, T., Synthesis of a C-N Axially Chiral *N*-Arylisatin through Asymmetric Intramolecular *N*-Arylation. *Eur. J. Org. Chem.* **2015**, 4603-4606.

(13) Asano, S.; Takahashi, Y.; Maki, T.; Muranaka, Y.; Cherkasov, N.; Mae, K., Contactless Mass Transfer for Intra-droplet Extraction. *Sci. Rep.* **2020**, *10*, 7685. The developed software in this work can be downloaded with detailed operation procedure at https://github.com/ShusakuASANO/KYOCHAN_Chiral.

(14) Regueira, T.; Yan, W.; Stenby, E. H., Densities of the Binary Systems *n*-Hexane plus *n*-Decane and *n*-Hexane plus *n*-Hexadecane up to 60 MPa and 463 K. *J. Chem. Eng. Data* **2015**, *60*, 3631-3645.

(15) The enantiomeric excess values of the samples were determined by UV signal of PDA detector to avoid the influence of artifacts of CD detector.

(16) The range of $\Delta H_{rac}^{\ddagger}$ and $\Delta S_{rac}^{\ddagger}$ are 26.9-27.8 kcal·mol^{-1} and 5.04-7.72 cal·mol^{-1}·K^{-1}, respectively, in consideration of the SE of Eyring plot.

(17) **2a** was newly synthesized in this study. See, the Supporting Information for the detail of the synthesis.

(18) Garcia-Miaja, G.; Troncoso, J.; Romani, L., Density and Heat Capacity as a Function of Temperature for Binary Mixtures of 1-Butyl-3-methylpyridinium Tetrafluoroborate plus Water, plus Ethanol, and plus Nitromethane. *J. Chem. Eng. Data* **2007**, *52*, 2261-2265.

(19) The range of $\Delta H_{rac}^{\ddagger}$ and $\Delta S_{rac}^{\ddagger}$ are 25.4-26.1 kcal·mol^{-1} and 2.49-4.39 cal·mol^{-1}·K^{-1}, respectively, in consideration of the SE of Eyring plot.